Supplemental Document

Optics EXPRESS

Optical memories and switching dynamics of counterpropagating light states in microresonators: supplement

LEONARDO DEL BINO,[1,2,3] NIALL MORONEY,[1,2,4] AND PASCAL DEL'HAYE[1,2,*]

[1]*Max Planck Institute for the Science of Light, Staudtstraße 2, 91058 Erlangen, Germany*
[2]*National Physical Laboratory, Hampton Road, Teddington, TW11 0LW, United Kingdom*
[3]*Heriot-Watt University, Edinburgh, EH14 4AS, Scotland, United Kingdom*
[4]*Imperial College London, London, SW7 2AZ, United Kingdom*
[*]*pascal.delhaye@mpl.mpg.de*

Supplement DOI: https://doi.org/10.6084/m9.figshare.13469109

Parent Article DOI: https://doi.org/10.1364/OE.417951

Optical memories and switching dynamics of counterpropagating light states in microresonators: supplemental document

1. RESONATOR FABRICATION

The microresonator is fabricated from a 3-mm-diameter silica rod by spinning it on a spindle and using a 100 W CO_2 laser to ablate the surface down to 2.7 mm diameter and create the resonator profile. Finally, the surface is annealed at lower power to achieve high Q-factor[1].

2. EOM OVERDRIVE

Being able to change the input power much faster than the response of the cavity allows us to consider the input modulation as an instantaneous change in power instead of considering the output as a convolution between the drive and the response. This simplifies the mathematical approach and the simulations, and makes the experimental results easier to understand. In the experiments we use an EOM to modulate the power faster than the cavity lifetime ($\gtrsim$ 165 ns). However, EOMs respond in a particular way: about one third of the modulation is almost instantaneous with the driving voltage (10 GHz bandwidth), but the other two thirds are governed by charge accumulation and polarization of the electro-optic crystal that takes place over a few microseconds. Since we need flat HIGH and LOW power levels for this experiment we need to correct for this effect. To do so, we measure the transmission of the EOMs with a Heaviside function voltage input and fit the response with an instantaneous component and three exponentially decaying terms with free time constants and weights. This fit is then used to calculate the input voltage profile that would produce the desired transmission response. This results in a rise time of 8 ns even for full-range modulations, and a high level which is defined within 2 % power fluctuations after the switching.

3. DATA FOR SIMULATIONS

The traces in Figure 6 in the main article are generated using the parameters in Table S1. The Q-factor, diameter and A_{eff} for the "SiO_2 rod" are the ones measured and calculated for the resonator used in this work. For chip-based SiO_2 toroid resonators we use results from resonators fabricated in our group [2]. The parameters for the other materials are instead collected from other recent works.

4. OTHER PARAMETERS AFFECTING THE SWITCHING

The modulation amplitude is the most important parameter affecting the switching speed, but the laser detuning and the total input power also have a small effect on the switching profile. Fig. S1 shows how the power affects the switching profile. The rise time varies by about 30 % over the range of input powers considered. Also, a clear overshoot and ringdown arise at higher powers, whose magnitude and frequency become higher as the power increases.

5. INPUT SIGNALS

Fig. S2 shows the input powers used to measure the hysteresis profiles displayed in Figure 3 in the main article. Notice how the total power sent to the resonator is constant and the ramp takes place on a timescale much longer than the switching speed.

The input power used to measure and simulate the switching profile in Figure 4 in the main article is shown in Fig. S3. Each cycle starts with a reset phase (a) when the power is imbalanced enough to overcome the hysteresis and bring the red direction to the LOW state. The powers are

Table S1. Parameters used for the simulation in Figure 6 in the main article. * For silicon a wavelength of 3.1 µm is used insted of 1.55 µm. A_{eff} is the effective mode area, n is the refractive index, n_2 is the nonlinear refractive index, and Q_0 is the intrinsic Q-factor.

Material	diam.	A_{eff}	n	n_2 [cm^2/W]	Q_0
SiO_2 rod	2 mm	50 µm^2	1.444	2.7×10^{-16} [3]	4×10^8
SiO_2 toroid	100 µm	4 µm^2	1.444	2.7×10^{-16}	7×10^7
Si_3N_4 [4]	600 µm	1 µm^2	2.463	2.4×10^{-15}	1.7×10^7
CaF_2 [5]	6 mm	20 µm^2	1.426	1.9×10^{-16}	3×10^9
MgF_2 [5]	2 mm	20 µm^2	1.37	9×10^{-17}	1×10^9
Si* [6]	100 µm	1 µm^2	3.43	1.7×10^{-14} [7]	7×10^5

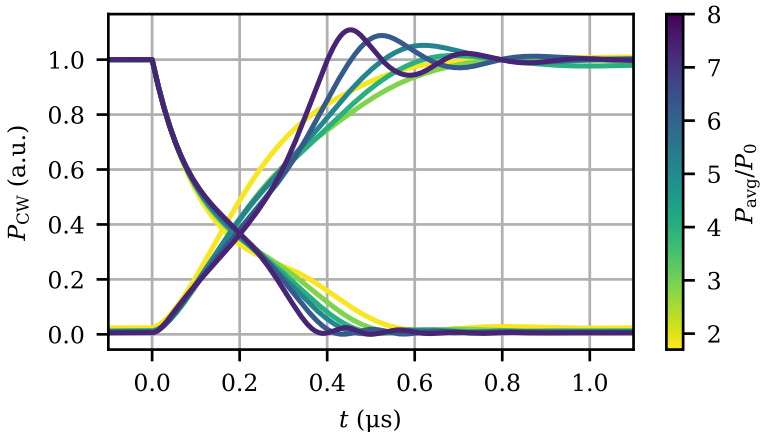

Fig. S1. Simulation of the switching profile for different input powers. The average input power range from $P_{\text{in}} = 1.7P_0$ to $P_{\text{in}} = 8P_0$.

then returned to near equality (10 % imbalanced) and this constitutes the initial state (b). Finally, the powers are imbalanced to the final state (c) and the temporal profile of the coupled power in the red direction is measured. The amount of imbalance in the final phase indicated by the arrow in Fig. S3 is varied from 0 to 100 % of the average power over 200 cycles. Some of the cycles are plotted in Figure 4 in the main article with the relative imbalance shown by the color of the line.

The input signals for Figure 5 in the main article and Fig. S1 are random sequences of bits with square wave transitions between high and low levels. The two inputs are switched in opposite directions such that the total input power is constant.

6. COUPLING AND Q-FACTOR

To obtain the curves in Figure 6 in the main article, we compare the threshold power P_{th} defined in Equation (S3), and the bitrate R defined in the main article. The coupled Q-factor is a common element between both equations. It is defined from the intrinsic linewidth γ_0 and the coupling strength κ as follows:

$$Q_0 = \frac{\omega}{2\gamma_0}; \qquad Q = \frac{\omega}{2\gamma}. \tag{S1}$$

Where $2\pi\omega$ is the the optical frequency. The coupling efficiency, i.e. the maximum fraction of light that can get transferred from the tapered fiber to the resonator, is expressed as

$$\eta = \frac{4\kappa\gamma_0}{\gamma^2}, \tag{S2}$$

where the coupled linewidth is $\gamma = \kappa + \gamma_0$. The maximum coupling efficiency $\eta = 1$ is obtained for $\kappa = \gamma_0$.

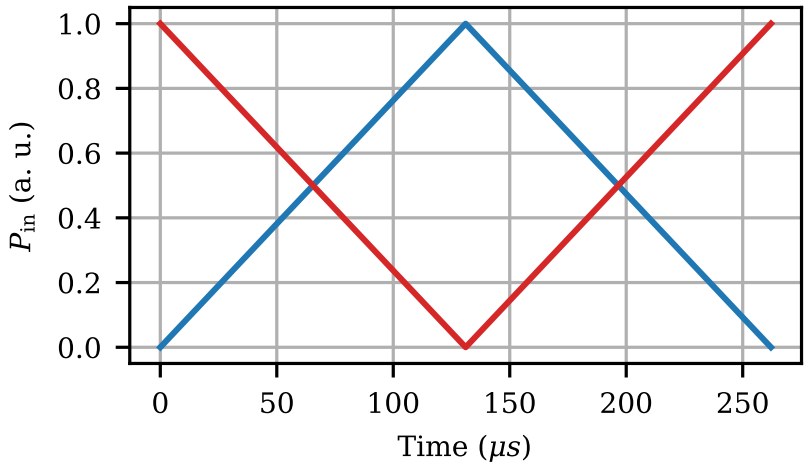

Fig. S2. Input power profile in the two directions (blue and red) used in Figure 3 in the main article.

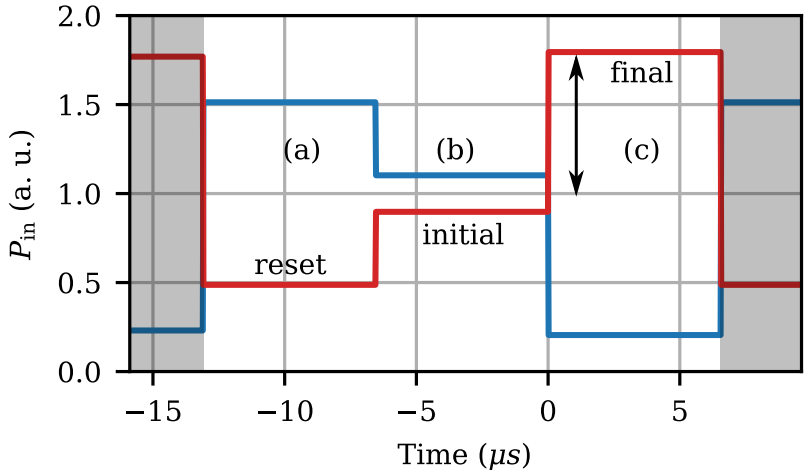

Fig. S3. A cycle of the input power profile in the two directions (blue and red) used in Figure 4 in the main article. The origin of the time scale is the same here as in Figure 4. The three phases of the cycle are marked and the variable part is highlighted by an arrow.

For each type of resonator a compromise between speed and power consumption is chosen by tuning the coupling of the resonator with the input/output waveguide. In Figure 6 in the main article, the parameter κ varies from $0.03\gamma_0$ to $30\gamma_0$ and the corresponding threshold power, and bitrate are plotted.

$$P_{\mathrm{th}} = \frac{1.54}{\eta} \frac{\pi^2 n_0^2 d A}{n_2 \lambda Q(\kappa) Q_0}, \tag{S3}$$

$$R = \frac{1}{2.197} \frac{\omega}{Q(\kappa)} \tag{S4}$$

REFERENCES

1. P. Del'Haye, S. A. Diddams, and S. B. Papp, "Laser-machined ultra-high-Q microrod resonators for nonlinear optics," Appl. Phys. Lett. **102**, 221119 (2013).
2. S. Zhang, J. M. Silver, L. Del Bino, F. Copie, M. T. M. Woodley, G. N. Ghalanos, A. Ø. Svela, N. Moroney, and P. Del'Haye, "Sub-milliwatt-level microresonator solitons with extended access range using an auxiliary laser," Optica **6**, 206 (2019).

3. T. Kato, Y. Suetsugu, M. Takagi, E. Sasaoka, and M. Nishimura, "Measurement of the nonlinear refractive index in optical fiber by the cross-phase-modulation method with depolarized pump light," Opt. Lett. **20**, 988–990 (1995).
4. Y. Xuan, Y. Liu, L. T. Varghese, A. J. Metcalf, X. Xue, P.-H. Wang, K. Han, J. A. Jaramillo-Villegas, A. A. Noman, C. Wang, S. Kim, M. Teng, Y. J. Lee, B. Niu, L. Fan, J. Wang, D. E. Leaird, A. M. Weiner, and M. Qi, "High-q silicon nitride microresonators exhibiting low-power frequency comb initiation," Optica **3**, 1171 (2016).
5. A. A. Savchenkov, D. Eliyahu, W. Liang, V. S. Ilchenko, J. Byrd, A. B. Matsko, D. Seidel, and L. Maleki, "Stabilization of a kerr frequency comb oscillator," Opt. Lett. **38**, 2636 (2013).
6. M. Yu, Y. Okawachi, A. G. Griffith, M. Lipson, and A. L. Gaeta, "Mode-locked mid-infrared frequency combs in a silicon microresonator," Optica **3**, 854 (2016).
7. Q. Lin, J. Zhang, G. Piredda, R. W. Boyd, P. M. Fauchet, and G. P. Agrawal, "Dispersion of silicon nonlinearities in the near infrared region," Appl. Phys. Lett. **91**, 021111 (2007).